

1 Introduction

The aim of this project is to design, calibrate, and validate a simple low-cost sun radiometer. We follow the method proposed by Forrest Mims [1] which consists of using a light-emitting diode (LED) as a low-cost detector and optical filter. The LED acts as a photovoltaic (PV) detector whose short-circuit current (photocurrent) is proportional to the Sun's irradiance. This current and, thus, the voltage it generates are amplified by a transimpedance amplifier, as shown in Fig. 1.

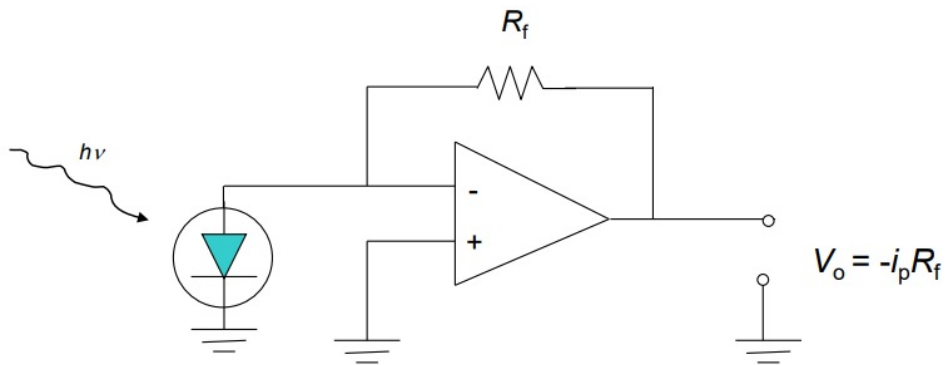


Figure 1: Solar radiometer circuit [2]

The remainder of this report is structured as follows: In Section 2, we provide a brief explanation of the implementation and automation of the solar radiometer device. Section 3 provides details about the data collected. Section 3 presents the calibration and prediction results, and Section 5 shows the calculation of the aerosol optical depth. Finally, Section 6 offers comparison results to the MODTRAN software.

2 Device Specifications

The architecture of the proposed system was designed in Solidworks and consists of two degrees of freedom, as shown in Fig. 2. The tube of this system is designed to house an LED diode that is used as our sensor. The length of the tube allows the sensor to have a narrow aperture angle of 3° approximately in order to measure direct radiation only and avoid the interference of diffused radiation [3]. The LED acts as a PV detector and its short-circuit current is amplified by an operational amplifier (LM324) using a feedback resistor $R_f = 4M\Omega$. The amplified signal (voltage) is automatically read by an Arduino UNO. The amplifier circuit uses a voltage source of $\pm 9V$ while the servomotors are powered with a separate voltage source of $5V$. The implemented device is shown in Fig. 3. Note that Fig. 3 shows that a red LED was used for initial experiments; however, a green LED (550 nm) was used to collect the data used in this report.

The position of the tube is controlled by two servo motors, whose angles are calculated by the Arduino. More specifically, the purpose of the Arduino program is to align the tube with the position of the Sun thorough the day; that is, it calculates the Sun's azimuth and zenith angles constantly. More details are provided in Algorithm 1¹, where `getZenith()` and `getAzimuth()` are two functions that take as input the current time and the GPS position to calculate the Sun's azimuth and zenith angles; `servo.write(X)` is a function that moves a servo X° ; and `gridSearch()` is a function that moves the tube $\pm(3, 3)^\circ$ around the calculated position reading the voltage from the sensor with a step of 0.5° (at each position, the voltage reading is reading 10 times and averaged to reduce uncertainty) and retrieving the maximum voltage reading.

Algorithm 1 Arduino pseudocode

```
1: function SOLARRADIOMETER
2:   while True do
3:     // Step 1: Calculate solar angle (zenith and azimuth).
4:     zenith = getZenith()
5:     azimuth = getAzimuth()
6:     // Step 2: Move servos to the calculated position.
7:     servobase.write(azimuth) // Moves servo 1
8:     servoled.write(zenith) // Moves servo 2
9:     // Step 3: Perform a grid search around the current position to find the max. voltage.
10:    maxV = gridSearch()
11:    // Step 4: Save voltage measurement in a CSV file.
12:    save(Zenith, azimuth, maxV)
13:    delay(60000) // Repeat each minute
14:  return False
```

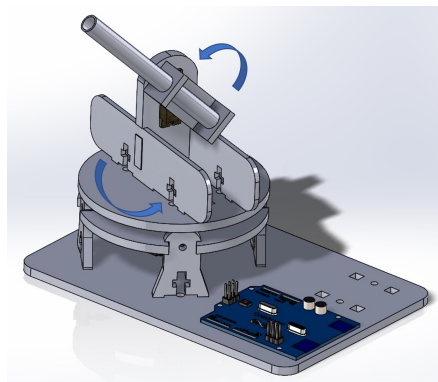


Figure 2: Architecture design in Solidworks.

¹Videos, images, and all scripts and files used in this project are available at: <https://github.com/GiorgioMorales/SolarRadiometer>



Figure 3: Left: Implemented solar radiometer device. Right: LED located inside the tube and powered with 3.3 V to demonstrate a well-functioning connection.

Table 1: Data Acquisition Conditions

	March 22	March 23
Sky condition	Clear sky	Mostly clear with occasional clouds
Adquisition time	3:47 - 6:30 pm	7:56 - 10:30 am
Average Temperature	50 °F	40 °F
Pressure	843 hPa	839.9 hPa

3 Data Collection

Two days were used for data collection: March 22nd and March 23rd, 2022. All data points were read from the same location (Cobleigh Hall's roof, Bozeman, Montana). Table 1 shows the acquisition conditions of these days. Moreover, Fig. 4 and Fig. 5 show the voltage readings with their corresponding acquisition time (in UTM time). Note that some of the perturbations were due to cloud occlusion and most of them were photographed. Another source of uncertainty is the constant movement of the tube and, thus, the LED during the grid search process.

4 Data Processing

The collected data is used to create a calibration Langley plot, which consists of plotting the natural logarithm of the detector voltage as a function of air mass. The acquisition hour is used to calculate the zenith angle θ_z , which, in turn, is used to calculate the air mass through the following equation that takes into account refraction compensation [4]:

$$M(\theta_z) = \frac{1.002432 \cos(\theta_z)^2 + 0.148386 \cos(\theta_z) + 0.0096467}{\cos(\theta_z)^3 + 0.149864 \cos(\theta_z)^2 + 0.0102963 \cos(\theta_z) + 0.000303978}.$$

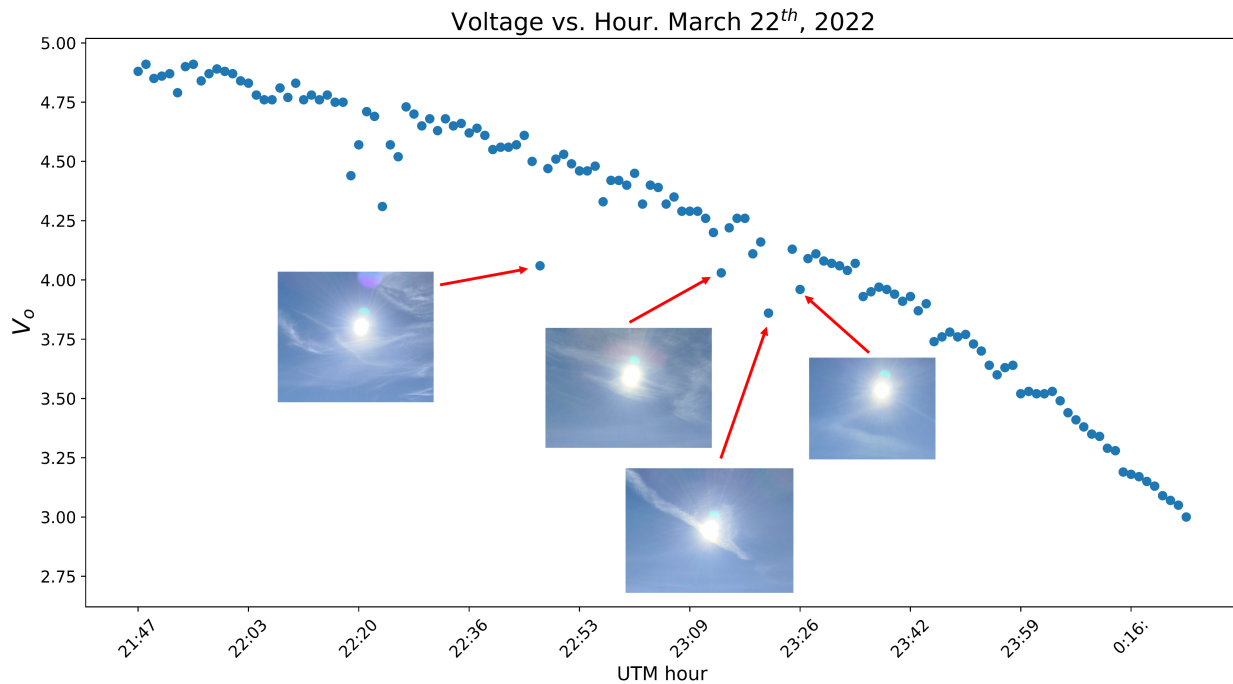


Figure 4: Data collected on March 22nd, 2022.

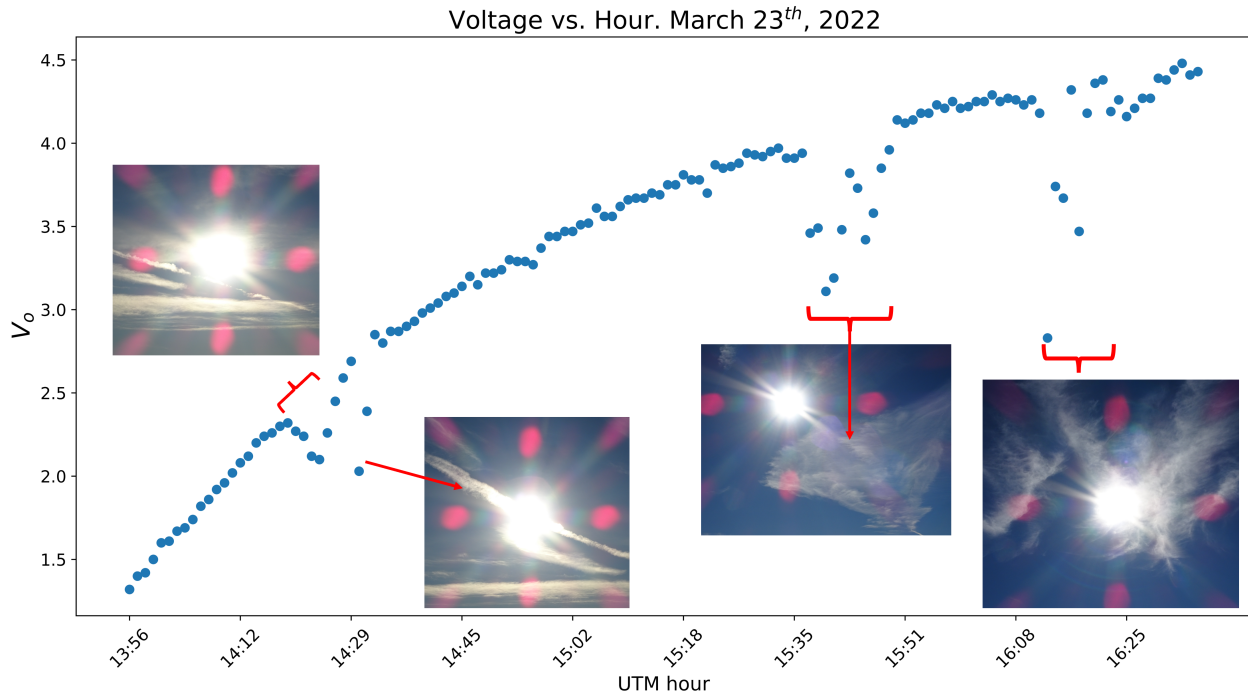


Figure 5: Data collected on March 23rd, 2022.

According to the Beer-Bouguer-Lambert law, the irradiance of a light beam at wavelength λ is reduced exponentially with distance [2]:

$$\text{Spectral irradiance} = E(\lambda) = E_0(\lambda)e^{-\tau(\lambda,\theta_z)}, \left[\frac{W}{m^2 nm} \right] \quad (1)$$

where $\tau(\lambda, \theta_z)$ represents the optical depth and $E_0(\lambda)$ is the initial spectral irradiance at wavelength λ . We also consider that the optical depth is proportional to the air mass:

$$\tau(\lambda, \theta_z) = \tau M(\theta_z), \quad (2)$$

where τ represents the optical depth of the atmospheric path ($\theta_z = 0$). The solar irradiance is not directly measured by our PV detector; however, its detected voltage, V_d , is proportional to $E(\lambda)$ ($V_d \propto E(\lambda)$), from which we have that:

$$V_d = V_0 e^{-\tau(\lambda, \theta_z)} = V_0 e^{-\tau M(\theta_z)},$$

and V_0 indicates the ideal voltage that would be read by the detector at $M(\theta_z) = 0$ (proportional to the exo-atmospheric irradiance). Taking the logarithm of both sides of the previous equation, we get:

$$\ln(V_d) = -\tau M(\theta_z) + \ln(V_0). \quad (3)$$

Thus, the variables τ and V_0 can be fit from data using Eq. 3 through a simple linear regression model. Fig. 6 shows the Langley plots obtained from the collected data as well as their corresponding fitted linear equations. From Fig. 6.a, we obtained an **optical depth of** $\tau = 0.1695$ whereas, from Fig. 6.b, we obtained an **optical depth of** $\tau = 0.1592$. Note that the data from March 23rd was fitted including air mass values greater than 6 (i.e., at zenith angles greater than 80°), which increases uncertainty in the measurements. However, the diversity of points collected the second day is greater than in the first day and might provide a better optical depth estimation. For instance, in Fig. 6.a, we notice that the set of points with an air mass between 4 and 5 slightly deviate (and, hence, increase) the slope of the fitted hyperplane, which justifies the difference between the optical depth calculated from the two consecutive days.

We can also use the data captured on March 22nd for calibration while the data captured on March 23rd is used for validation. Considering that these data sets correspond to two consecutive days, the calibration constant is almost 1 (more precisely, 0.99961) because their corresponding Earth-Sun distances are similar. Fig. 7 shows the comparison between the data predicted on March 23rd using the calibration from March 22nd versus the actual data captured on March 23rd. The calculated root mean square (RMSE) value is $RMSE = 0.00172$.

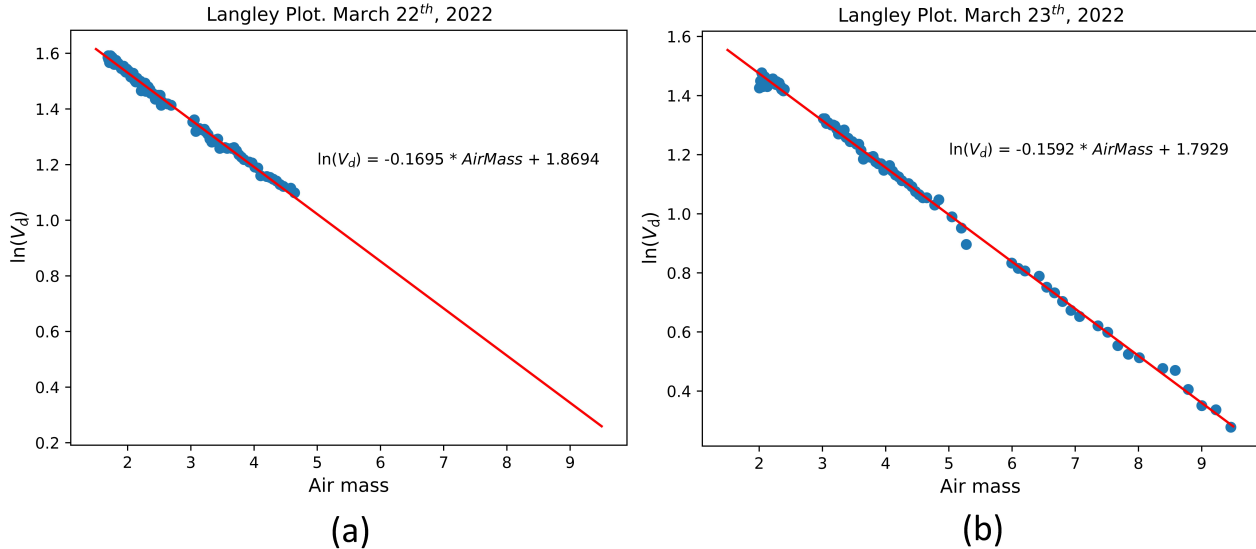


Figure 6: Langley Plots fitted using data from (a) March 22 and (b) March 23.

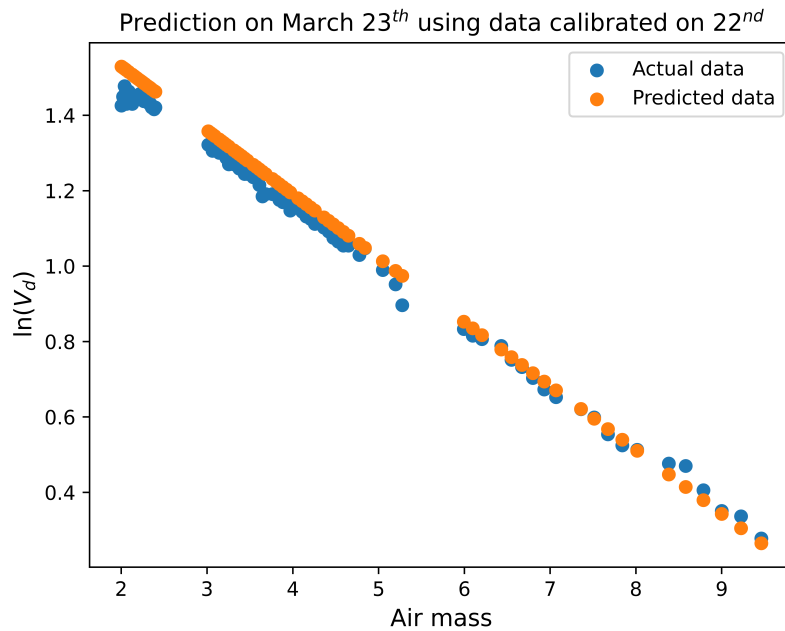


Figure 7: Data predicted on March 23rd using the calibration from March 22nd.

5 Aerosol Optical Depth Calculation

So far, we have considered the total optical depth τ . Nevertheless, τ encompasses the effect of several components [3]:

$$\tau = \tau_{AOD} + \tau_{RS} + \tau_G, \quad (4)$$

where τ_{AOD} denotes the aerosol optical depth, τ_{RS} denotes the Rayleigh optical depth, and τ_G denotes the optical depth due to absorption by gases, where O_3 has the most impact. In this work, we will ignore the effect of absorption by gases ($\tau_G \approx 0$) considering that there is little molecular absorption in the visible spectral range and transmittance is limited primarily by scattering [5].

The Rayleigh optical depth is calculated using the following approximation function given by Dutton et al. [6]:

$$\tau_{RS} = 0.00877 \frac{P}{P_0} \lambda^{-4.05}, \quad (5)$$

where P denotes the site pressure, P_0 is the atmospheric pressure at sea level (1013.25 hPa), and λ is the wavelength in micrometers. This equation was fitted for the visible range and does not behave well in other parts of the spectrum [7]; however, considering that we are working with a green LED ($\lambda = 525$ nm), Eq. 5 is enough for this study. Hence, replacing the P values during our collection campaign from Table 1 we obtain the Rayleigh optical depth:

$$\text{March } 22^{\text{nd}}: \tau_{RS} = 0.1031,$$

$$\text{March } 23^{\text{rd}}: \tau_{RS} = 0.1027.$$

Therefore, the aerosol optical depth is calculated as:

$$\text{March } 22^{\text{nd}}: \tau_{AOD} = \tau - \tau_{RS} = 0.1695 - 0.1031 = \mathbf{0.04834},$$

$$\text{March } 23^{\text{rd}}: \tau_{AOD} = \tau - \tau_{RS} = 0.1592 - 0.1027 = \mathbf{0.05647},$$

In addition, the maximum τ_{AOD} reported by the Montana State University Aeronet instrument (see Fig. 8) is approximately **0.033** for a similar wavelength between February 1st and February 19th (the most recent reported dates). We argue that the aerosol optical depth in March should be similar and slightly higher than that captured in February. Therefore, we claim that our results are consistent with those obtained by of Aeronet considering that the increment is lower than 0.03.

6 MODTRAN Comparison

We used MODTRAN5 to validate our results. In particular, we estimate transmittance values using the following parameters (which are also shown in Fig. 9):

- Model atmosphere: Mid-latitude Winter.

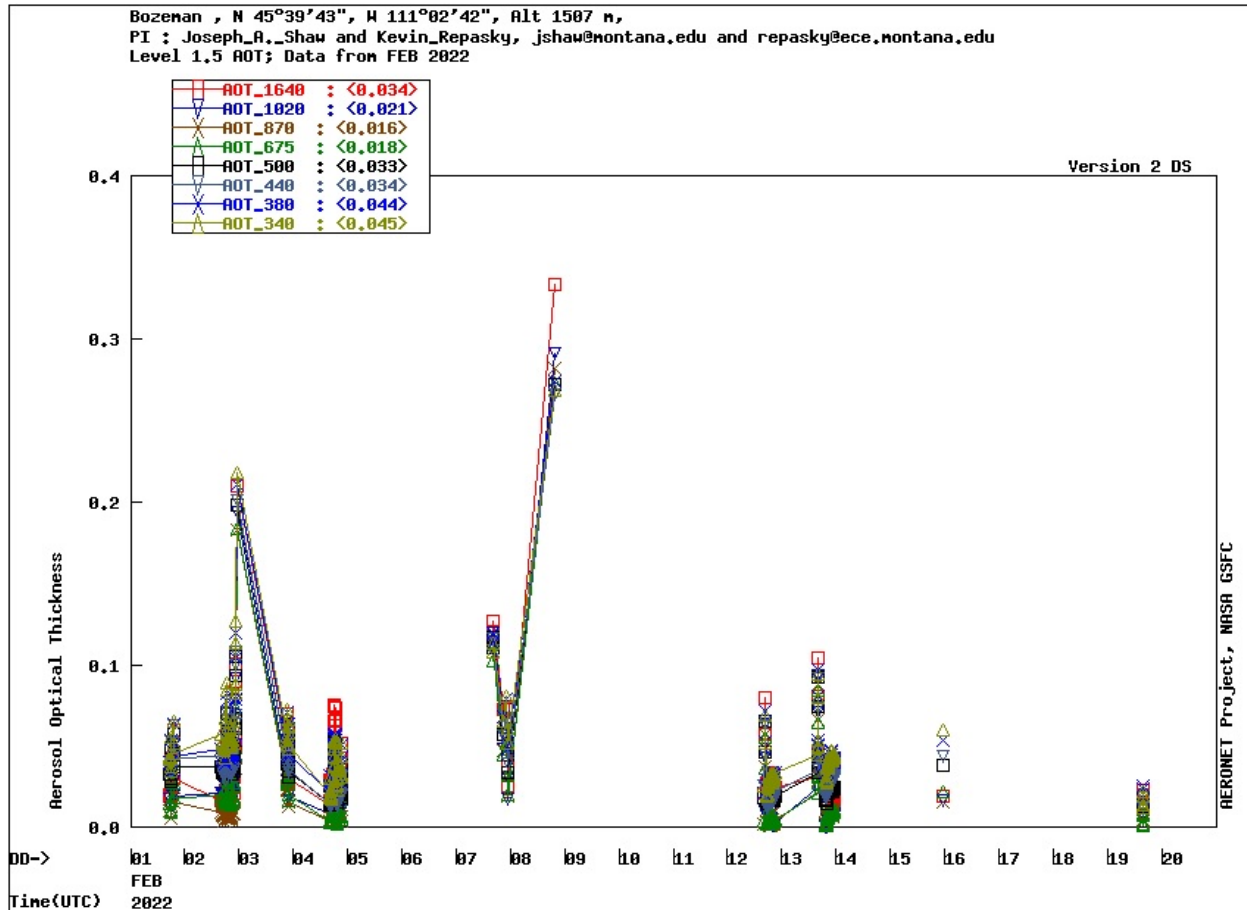


Figure 8: Aerosol optical depth measured by the Montana State University Aeronet instrument.

- Type of atmospheric path: Slant Path to Space or Ground.
- Path Type: Observer height, zenith angle
- CO₂ Mixing Ratio: 400 ppmv.
- Aerosol Mode Used: “No aerosols or clouds” (to calculate the lower bound) and “Rural - VIS = 23km” (for estimations including aerosol effect).
- Ground altitude above sea level: 1.5km.
- Initial Frequency: 520 nm.
- Final Frequency: 550 nm.

As mentioned above, we used two aerosol modes. The first one is the “No aerosols or clouds”, which estimates total transmittance values within the specified wavelengths assuming there

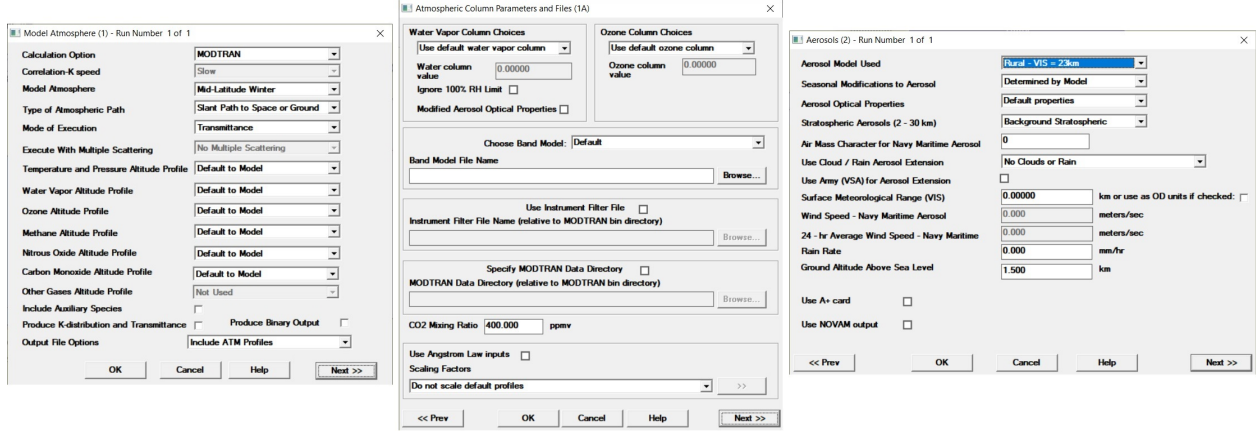


Figure 9: Configuration parameters used in MODTRAN.

are no aerosol or clouds in the atmosphere. This mode will provide us with a lower bound for our optical depth calculations. We also used the “Rural - VIS = 23km” mode because it considers similar conditions to those of Bozeman, MT. Thus, we expect the results of this mode to be similar to ours (reported in Sec. 4). Fig. 10 shows an example of a transmittance plot obtained using the the “Rural - VIS = 23km” mode.

Similar to what was explained in Sec. 4 using Eq. 1- 1, we consider that the transmittance, T , is proportional to $E(\lambda)$, from which we have that:

$$\ln(T) = -\tau M(\theta_z) + \ln(T_0). \quad (6)$$

Using MODTRAN, we calculate the average transmittance values within the specified wavelength range for five zenith angles: 0° , 20° , 40° , 60° , and 80° . Tables 2 and 3 show the estimated transmittance values using both modes. Then, we used the estimated values to fit a linear regression model based on Eq. 6. Fig. 11 depicts the Langley plots and their corresponding fitted linear equations. Hence, we obtain an **optical depth** of $\tau_{NoAOD} = 0.049$ for the “No aerosol or clouds” mode (Fig. 11.a). Likewise, we obtain an **optical depth** of $\tau_{Rural} = 0.1592$ for the “Rural - VIS = 23km” mode (Fig. 11.b).

Now validate our empiric results by comparing them with those estimated by MODTRAN. The optical depths we obtained from March 22nd and March 23rd were $\tau = 0.1695$ and $\tau = 0.1592$. Both were greater than τ_{NoAOD} ($0.1695 > 0.049$ and $0.1592 > 0.049$), which is consistent with the fact that the optical depth is expected to increase due to the presence of aerosol. Moreover, our estimated optical depths were similar to τ_{Rural} ($0.1695 \approx 0.1592$ and $0.1592 \approx 0.1592$). Note that the optical depth we obtained from March 23rd (i.e., the date where more data points were captured) was practically the same as that estimated by MODTRAN.

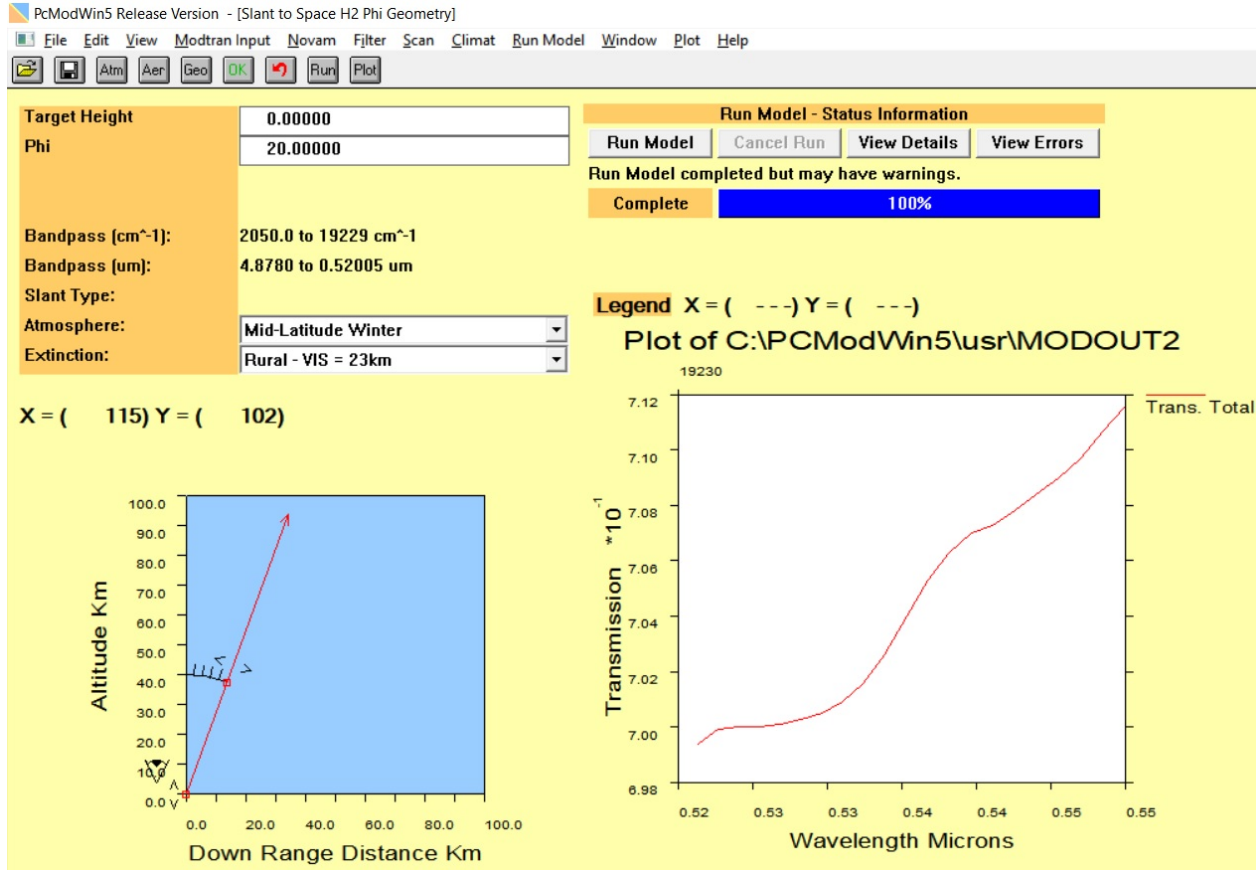


Figure 10: Example of a transmittance plot obtained with MODTRAN.

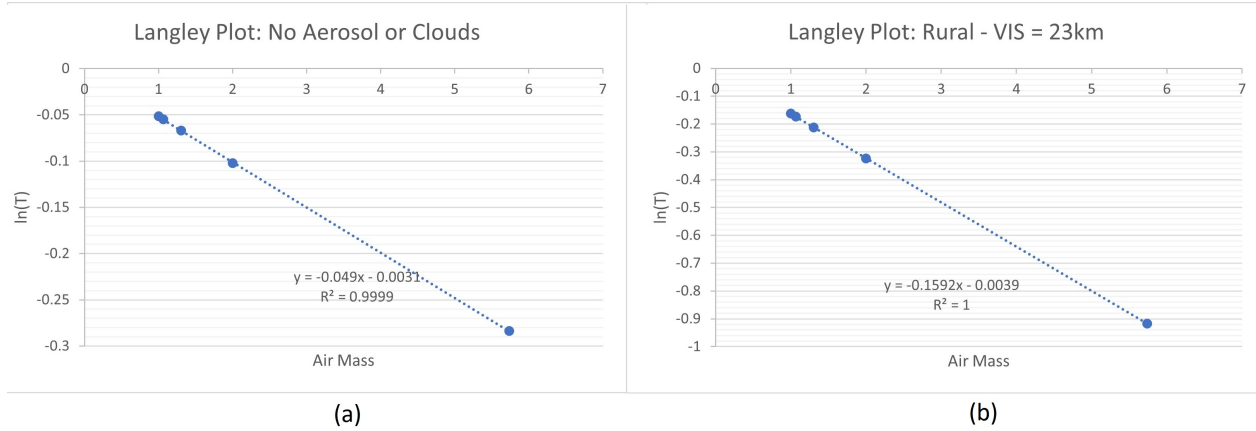


Figure 11: Example of a transmittance plot obtained with MODTRAN.

References

- [1] Forrest M. Mims. Sun photometer with light-emitting diodes as spectrally selective detectors. *Appl. Opt.*, 31(33):6965–6967, Nov 1992.

Table 2: MODTRAN results using the “No Aerosol or Clouds” mode.

Zenith	Transmission	Air mass	Ln(T)
0	0.888	1	-0.05159
20	0.88164	1.064109251	-0.05471
40	0.856944	1.305019811	-0.06705
60	0.789964	1.998162933	-0.10239
80	0.520184	5.735746374	-0.28384

Table 3: MODTRAN results using the “Rural - VIS = 23km ” mode.

Zenith	Transmission	Air mass	Ln(T)
0	0.68824	1	-0.16226
20	0.671964	1.064109251	-0.17265
40	0.61418	1.305019811	-0.2117
60	0.474388	1.998162933	-0.32387
80	0.12118	5.735746374	-0.91657

- [2] Joseph Shaw. Lecture notes in remote sensing systems, EELE 583 - Spring 2022, Montana State University.
- [3] Glenn E. Shaw. Sun photometry. *Bulletin of the American Meteorological Society*, 64(1):4 – 10, 1983.
- [4] Andrew T. Young. Air mass and refraction. *Appl. Opt.*, 33(6):1108–1110, Feb 1994.
- [5] Joseph A Shaw and Paul W Nugent. Physics principles in radiometric infrared imaging of clouds in the atmosphere. *European Journal of Physics*, 34(6):S111, 2013.
- [6] Ellsworth G. Dutton, Patrick Reddy, Steve Ryan, and John J. Deluisi. Features and effects of aerosol optical depth observed at Mauna Loa, Hawaii: 1982-1992. *Journal of Geophysical Research*, 99(D4):8295–8306, April 1994.
- [7] Barry A. Bodhaine, Norman B. Wood, Ellsworth G. Dutton, and James R. Slusser. On rayleigh optical depth calculations. *Journal of Atmospheric and Oceanic Technology*, 16(11):1854 – 1861, 1999.